SCIENTIFIC REP**O**RTS

OPEN

Deep-Ultraviolet Photodetectors Based on Epitaxial ZnGa$_2$O$_4$ Thin Films

Si-Han Tsai[1], Sarbani Basu[1], Chiung-Yi Huang[1], Liang-Ching Hsu[2], Yan-Gu Lin[2] & Ray-Hua Horng [1,3]

A single-crystalline ZnGa$_2$O$_4$ epilayer was successfully grown on c-plane (0001) sapphire substrate by metal-organic chemical vapor deposition. This epilayer was used as a ternary oxide semiconductor for application in high-performance metal–semiconductor–metal photoconductive deep-ultraviolet (DUV) photodetectors (PDs). At a bias of 5V, the annealed ZnGa$_2$O$_4$ PDs showed better performance with a considerably low dark current of 1 pA, a responsivity of 86.3 A/W, cut-off wavelength of 280 nm, and a high DUV-to-visible discrimination ratio of approximately 10^7 upon exposure to 230 nm DUV illumination than that of as-grown ZnGa$_2$O$_4$ PDs. The as-grown PDs presented a dark current of 0.5 mA, a responsivity of 2782 A/W at 230 nm, and a photo-to-dark current contrast ratio of approximately one order. The rise time of annealed PDs was 0.5 s, and the relatively quick decay time was 0.7 s. The present results demonstrate that annealing process can reduce the oxygen vacancy defects and be potentially applied in ZnGa$_2$O$_4$ film-based DUV PD devices, which have been rarely reported in previous studies.

Recently, deep-ultraviolet (DUV, 190–350 nm) photodetectors (PDs) have attracted much attention due to their broad applications in the civil and military fields, such as engine control, solar UV monitoring, astronomy, lithography aligners, secure space-to-space communications, or missile detection[1–4]. These UV instruments are always operated at high temperature and harsh environments. Thus, several materials have been introduced to fabricate PDs. High photoresponsivity, low noise levels, high spectral selectivity, and high stability are required for PDs in such applications. Over the past decades, several semiconductor solar-blind PDs have obtained considerable achievements. A variety of well-established Si-based UV PDs are available in the market. However, UV-enhanced Si-based PDs exhibit limitations due to their low bandgap and requirement of expensive optical filters for spectral selectivity. Moreover, Si-based PDs efficiency can be degraded with increased temperature. To solve this problem, wide bandgap semiconductor materials, such as Group III nitrides: GaN, (Eg, ~3.4 eV) and AlN (~6.2 eV) and their ternary compounds, namely, Al$_x$Ga$_{1-x}$N (x > 40% with 6 eV) and SiC have been widely used for solar-blind and visible-blind UV PDs[5,6]. Nevertheless, high-density defects, such as dislocations and grain boundaries, can be generated during epitaxial growth of AlGaN films on sapphire substrate because of the lattice mismatch. On the other hand, persistent photoconductivity (PPC) effect also occurs when the free carrier density is equal to the trap density. Therefore, the most challenging aspects are to attain low dark current and high responsivity for the application of DUV PDs. Feng et al.[7] reported the first individual β-Ga$_2$O$_3$ nanowires as solar-blind PDs upon exposure to 254 nm light illumination; these nanowires present upper limits and response and recovery times of 0.22 and 0.09 s, respectively. Our previous studies also demonstrated the effects of crystallinity and point defects on the time-dependent photoresponsivity and cathodoluminescence (CL) properties of β-Ga$_2$O$_3$ grown by metalorganic chemical vapor deposition (MOCVD)[8]. PDs fabricated using 700 °C annealed β-Ga$_2$O$_3$ epilayers produced substantially low dark current of ~4 pA and large photocurrent-to-dark current contrast ratio of ~10^5 [8]. It is worthy to mention that ternary metal oxides have attracted significant attention due to its large bandgap and high wavelength selectivity. However, there is insufficient study regarding ternary metal oxide alloy PDs. Recently, Li et al. demonstrated an improved DUV-to-visible ratio of about 10^4, relatively fast response speed, low dark current of <0.1 pA, and a responsivity of 38.3 A/W (gain of ~200) for individual Zn$_2$GeO$_4$ nanowire visible-blind DUV PDs[9]. Our previous studies have also shown the high feasibility of single-crystalline spinel-shaped ZnGa$_2$O$_4$ films

^{1}Institute of Electronics, National Chiao Tung University, Hsinchu, 300, Taiwan, Republic of China. ^{2}National Synchrotron Radiation Research Center (NSRRC), Hsinchu, 300, Taiwan, Republic of China. ^{3}Center for Emergent Functional Matter Science, National Chiao Tung University, Hsinchu, 300, Taiwan, Republic of China. Correspondence and requests for materials should be addressed to R.-H.H. (email: rhh@nctu.edu.tw)
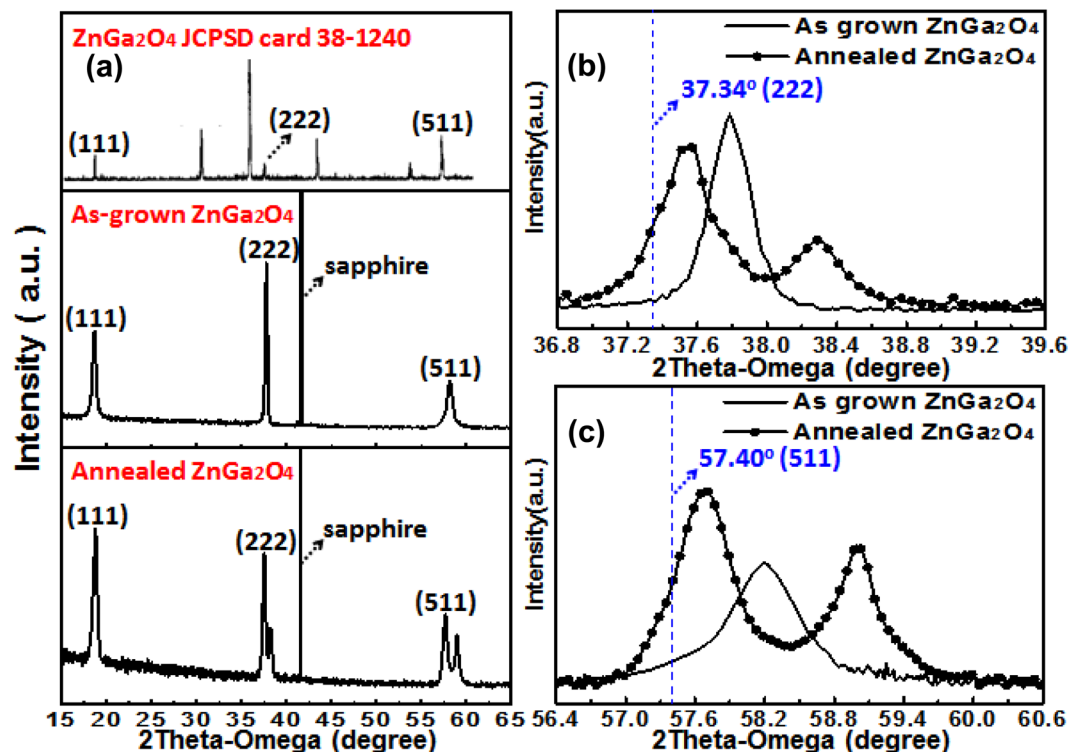
Figure 1. (**a**) Standard X-ray diffraction spectra of ternary compound $ZnGa_2O_4$ and the as-grown and annealed $ZnGa_2O_4$ thin films. (**b**) Diffraction peaks corresponding to the diffraction plane (111) of as-grown and annealed $ZnGa_2O_4$ thin films. (**c**) Diffraction peak corresponding to the diffraction plane (222) of as-grown and annealed $ZnGa_2O_4$ thin films.

prepared by MOCVD. These films have been fabricated to metal–oxide–semiconductor field-effect transistors[10]. The correlations among crystal, microstructural, morphological, compositional, CL, and electrical properties of these $ZnGa_2O_4$ films were also analyzed in details in our previous study[11]. The calculated carrier concentration, mobility, and resistivity of the $ZnGa_2O_4$ films were $6.72 \times 10^{16}\,cm^{-3}$, $1.4\,cm^2/Vs$, and $67.9\,\Omega\text{-cm}$, respectively. These values indicate that $ZnGa_2O_4$ films are promising for several optoelectronic applications[12]. In this work, the solar-blind PDs made of the $ZnGa_2O_4$ epilayers grown by MOCVD were studied. To further understand the annealing effect on the DUV PDs performance, as-grown and annealed PDs were also fabricated and their properties were studied in details. The corresponding crystalline, optical, and electrical properties of the $ZnGa_2O_4$ epilayers before and after thermal annealing were measured by X-ray diffraction (XRD) and X-ray photoelectron spectroscopy (XPS). The above properties related to the performance of DUV PDs were discussed in this paper.

Results and Discussion

The crystallinity of $ZnGa_2O_4$ films with and without thermal annealing was measured by XRD, as shown in Fig. 1(a). The crystal orientations of as-grown $ZnGa_2O_4$ films were characterized with evident XRD peaks at 18.67°, 37.77°, and 58.17°, which can be specified to (111), (222), and (511) diffraction planes. After furnace annealing treatment, the XRD peaks of $ZnGa_2O_4$ presented shifting phenomena. For comparison, the peaks of 18.40°, 37.34°, and 57.40° of standard $ZnGa_2O_4$ (JCPDS card 38–1240), which corresponded to (111), (222), and (511) diffraction planes of the cubic spinel crystal structure[13] was also shown in Fig. 1(a). In order to analysis more clearly, the peaks corresponding to the (222) and (511) diffraction planes were magnified and shown in Fig. 1(b,c). It was found that the XRD peaks corresponding to (222) diffraction plane for annealed $ZnGa_2O_4$ shifted from 37.77° to 37.55°. Similarly, the XRD peaks corresponding to (511) diffraction plane for annealed $ZnGa_2O_4$ shifted from 58.17° to 57.65°. These results indicated that the $ZnGa_2O_4$ film annealed in nitrogen ambient is close to the $ZnGa_2O_4$ cubic spinel structure. Moreover, the XRD peaks at approximately 38.25° and 59.01°, which were not observed in as-grown $ZnGa_2O_4$ film, were obtained in the annealed $ZnGa_2O_4$ thin film. They are the diffraction peaks of $\beta\text{-}Ga_2O_3$ monoclinic crystal structure. It means that the $(\bar{4}02)$ and $(\bar{6}03)$ diffraction planes for the standard $\beta\text{-}Ga_2O_3$ monoclinic crystal structure appeared in annealed film. This suggests that the recrystallization phenomenon made gallium and oxygen reorganize the $\beta\text{-}Ga_2O_3$ crystal through annealing process.

To further investigate the annealing effect in the $ZnGa_2O_4$ film, the surface morphologies (scanning length of $5\,\mu m$) of typical as-grown and annealed $ZnGa_2O_4$ films on sapphire were examined. The root-mean-square roughness values for the $ZnGa_2O_4$ films with and without annealing were 1.61 and 0.87 nm, respectively, as shown in Fig. 2(a,b). The annealed $ZnGa_2O_4$ film displayed relatively low surface roughness. The particle/agglomerate distribution was more uniform than that of the as-grown films. Therefore, annealing treatment resulted in smooth film surface. It is well known that the defects (e.g. oxygen vacancies and dangling bonds) always exist in the bulk
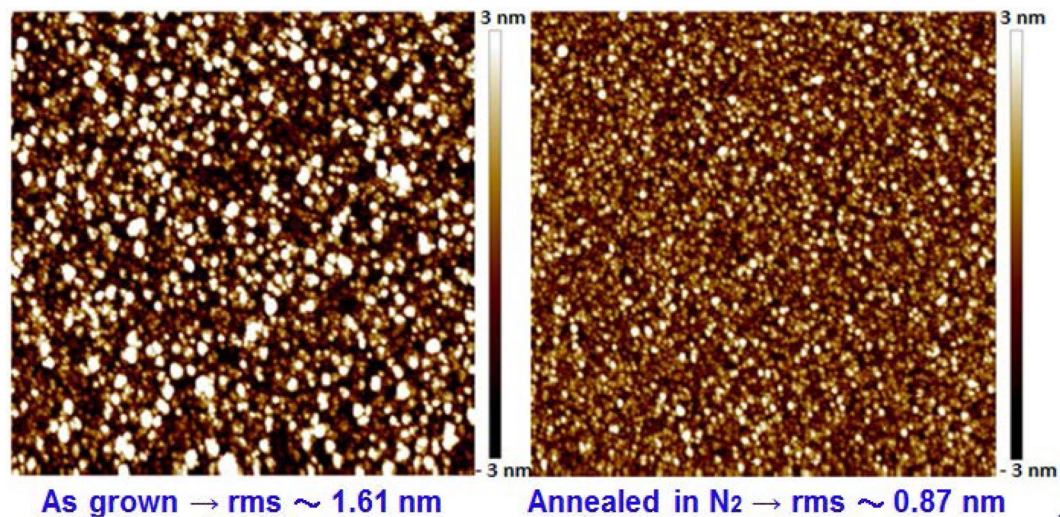
Figure 2. Atomic force microscope images of thin-film surfaces and surface roughness of as-grown and annealed $ZnGa_2O_4$ thin films.

and the surface of the epilayers. They were responsible in trapping the photogenerated electron or hole carriers. The smooth surface would lead to the low surface area and then the low surface density states for the annealed $ZnGa_2O_4$ film, which is beneficial for the improved performance of the PD[14,15].

XPS analysis can be used to characterize the surface chemical composition and bonding states of as-grown and annealed $ZnGa_2O_4$ films quantitatively. Figure 3(a,b) show the O1s core-level XPS spectra of as-grown and annealed $ZnGa_2O_4$ films, respectively. These XPS spectra were all fitted well with Gaussian functions. Figure 3(a,b) illustrate that the O1s core-level peaks of $ZnGa_2O_4$ (as-grown and annealed samples) can be divided into two components, namely, I and II, which were positioned at 530.78 and 532.10 eV, respectively. Peak I is assigned to lattice oxygen ions, and peak II is designated to the oxygen ions in the oxygen vacancies region[16]. Notably, the oxygen vacancy in an oxygen-deficient interlayer acted as an electron trap that can control the conductivity of oxide semiconductors[17]. Consequently, the oxygen vacancy proportion can correspond to conductive basis. The calculated area covered by the peak ratio of II/I was reduced from 0.167 to 0.11 after thermal annealing treatment. This result is consistent with the decrease in photocurrent after the annealing treatment[18].

The XANES shape of Ga K-edge spectra, which were dominated with geometry around Ga atoms, is shown in Fig. 4(a). The white-line feature and side hump are fitted to $ZnGa_2O_4$[19]. The adsorption edges of as-grown and annealed $ZnGa_2O_4$ were located at 10381.2 and 10380.7 eV, respectively. The white-line intensity of annealed sample was slightly lower than that of the as-grown one. The change and shifted energies of white-line feature can be attributed mainly to the disordered and different coordination environments[20]. In addition, the negative shift of the adsorption edge occurs with decreased coordination, which can be used as an indicator of the coordination number of O atom in the structure[21]. The Fourier transform EXAFS spectra of Ga K-edge were used to further understand the atomic structure of $ZnGa_2O_4$ film. Figure 4(b) shows the magnitude of the Fourier transforms of EXAFS functions. The first shell of Ga–O bonding (1–2 Å) slightly decreased after annealing treatment, which indicated the decreased coordination of O atoms. This phenomenon can be attributed to the decreased GaO_6 octahedron and GaO_3 tetrahedron ratio, which showed a trend similar to that of XANES results. Moreover, the annealed sample amplitudes showed a progressive decrease in the second shell due to the Ga–Ga bonding at 2–2.5 Å. By contrast, the Ga–Zn bonding amplitude (3–3.5 Å) was unaffected with the annealing treatment. This decrease in Ga–Ga amplitudes was caused by the disordered structure or phase transition between $ZnGa_2O_4$ and Ga_2O_3 as shown in Fig. 4(c). XAS results indicated that as-grown $ZnGa_2O_4$ was dominated with $ZnGa_2O_4$, and part of $ZnGa_2O_4$ structure may transform into Ga_2O_3 after annealing treatment. The obtained results well agreed with the observation found using XRD.

In this study, $ZnGa_2O_4$ epilayers displayed the wide bandgap (Eg, ~5.2 eV) responses to UV-C band (200–290 nm) and solar blindness to UV-A/B (290–400 nm). The bandgap measured by CL for the as-grown and annealed $ZnGa_2O_4$ epilayers have been discussed in the Supporting Text (Supplementary Information 1). Therefore, the $ZnGa_2O_4$ PD performance should be evaluated. I–V curves with and without UV illumination (DUV, 230 nm; power density, ~62.5 μW/cm^2) for PDs based on the as-grown and annealed $ZnGa_2O_4$ films are displayed in Fig. 5(a). The photocurrent increased with UV illumination or applied bias voltage for both devices at forward bias voltage due to the increased carrier drift velocity. This observation suggested that the films possessed photoconductive properties. Annealed $ZnGa_2O_4$ films presented a much lower dark current (Idark) at a bias of 20 V than that of the as-deposited films. The low dark current was attributed to the low concentration of the oxygen vacancies or low carrier density in the $ZnGa_2O_4$ films. Post-annealing affected the crystalline quality, surface properties, altered defects, and electrical properties of $ZnGa_2O_4$ films. Our previous studies have demonstrated the quality of as-grown $ZnGa_2O_4$ films, which contain lower degree of crystallinity and higher point defects than those of annealed $ZnGa_2O_4$ films[11]. The dark current of as-grown $ZnGa_2O_4$ film PDs (Idark ~1 mA at a 20 V bias)
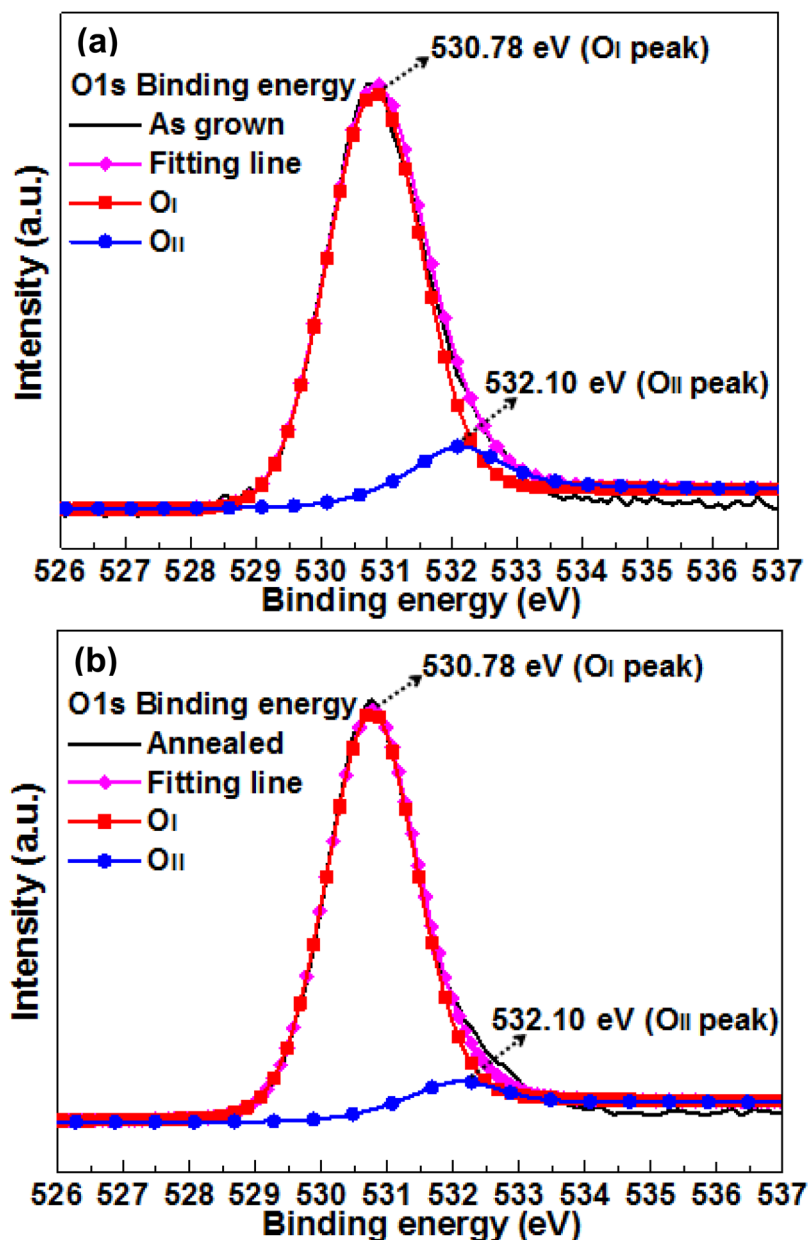
Figure 3. X-ray photoelectron spectroscopy spectra of O1s core level for (**a**) as-grown and (**b**) annealed $ZnGa_2O_4$.

was approximately 10^8 times higher than that of annealed PDs based on $ZnGa_2O_4$ films so that the photocurrent stimulated by DUV light was difficult to distinguish. High Idark for as-grown $ZnGa_2O_4$ films can be inter-related to the high intrinsic defects, such as oxygen vacancies and/or surface density state in the $ZnGa_2O_4$ films. The low photocurrent implied that the defect concentration was reduced, which resulted in low conductivity[15]. Surface-related defects can act as adsorption sites or trapping center to capture free electrons in $ZnGa_2O_4$ films. These trapping centers could result in current leakage. Therefore, the surface states enhance the current leakage and nonradiative recombination. Annealed $ZnGa_2O_4$ film-based detectors also showed low current leakage, which was below 1 pA, at 5 V reverse bias compared with those of as-grown counterparts due to the improved quality of material. Under a 230 nm (62.5 μW/cm^2) DUV illumination, the current increased by approximately one order of magnitude compared with that of the dark current for as-grown $ZnGa_2O_4$ PDs. However, the PDs made of annealed samples exhibited much higher photocurrent-to-dark current ratio of $\sim 10^8$, which is better than that of the reported MSM photodiodes[22–24].

Responsivity (R) is a significant detector parameter, which is defined as the ratio of the number of incident photons per incident optical power: $R = I_{ph}/P_{inc} = (I_{light} - I_{dark})/P_{inc}$, where P_{inc} is the incident optical power in watts, I_{ph} is the photocurrent. The plot of responsivity as a function of wavelength provided the spectral response of the detector. The PD responsivities with varying light intensities (~ 21.4, 40.2 and 62.5 μW/cm^2) as a function
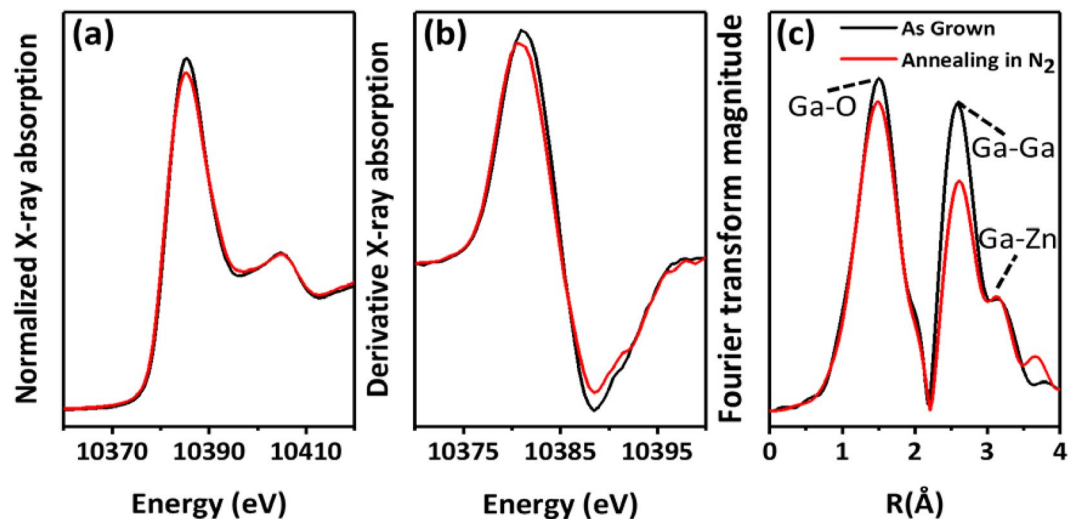
Figure 4. Ga K-edge (**a**) XANES, (**b**) derivative XANES, and (**c**) EXAFS spectra of $ZnGa_2O_4$.
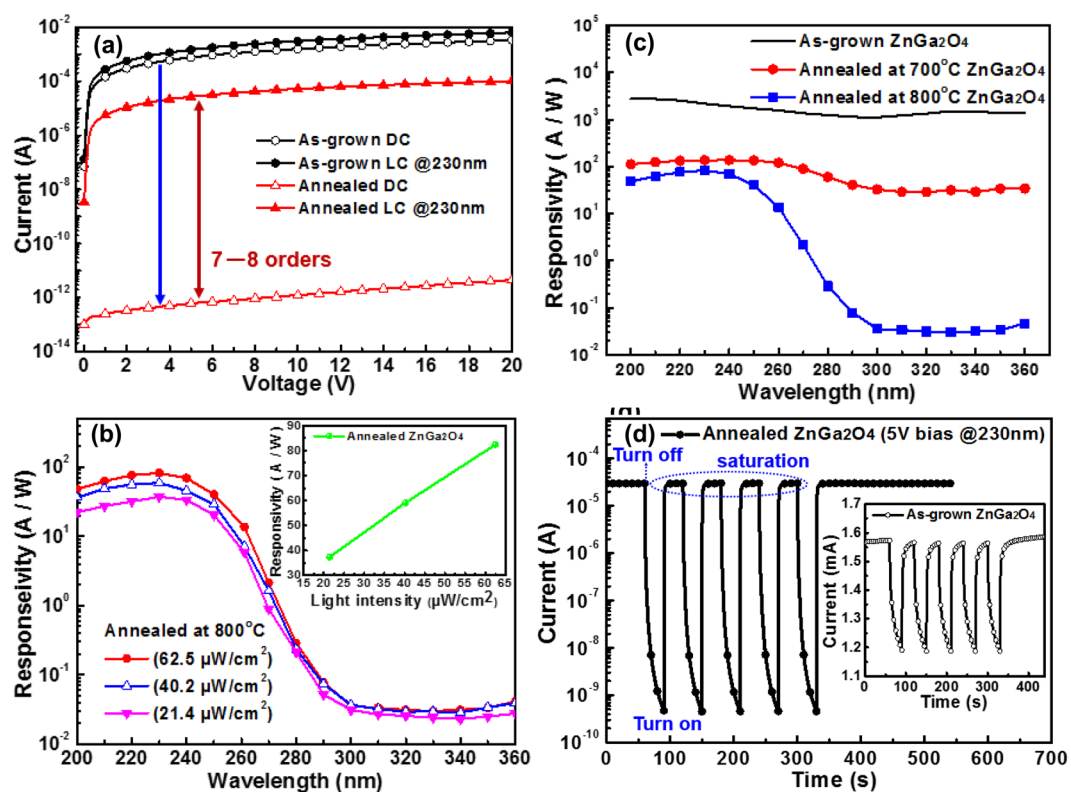

Figure 5. (**a**) Dark current (DC) curve and photocurrent (LC) at 230 nm curve for as-grown (black) and annealed in 800 °C (red) $ZnGa_2O_4$ UPDs. (**b**) Responsivity spectra of UV region for as-grown (black), annealed in 700 °C (red) and 800 °C (blue) $ZnGa_2O_4$ UPDs and the inset is the responsivity as a function of light intensity. (**c**) Spectral responsivities of MSM devices with varying light intensities (~21.4, 40.2 and 62.5 μW/cm²) of the N_2-annealed (800 °C) $ZnGa_2O_4$ UPDs at a 5 V bias. We have plotted Normalized responsivity (in logarithmic scale) to compare the out of band rejection ratio of the devices. The spectral responsivity measurement done by using a standard UV-enhanced Si Photodiode. After annealing, the solar blind selectivity of the $ZnGa_2O_4$ by 3 to 4 orders as compare to as-grown devices. (**d**) Dynamic photoresponse at 230 nm with 5 V bias of annealed (800 °C) $ZnGa_2O_4$ DUV PDs and the inset is the corresponding dynamic photoresponse of as-grown $ZnGa_2O_4$ DUV PDs.

of wavelength at an applied bias of 5 V for the $ZnGa_2O_4$ films annealed at 800 °C were investigated and shown in Fig. 5(b). Due to the light source limitations, the responsivity at a higher light intensity more than 62.5 μW/cm² cannot be measured. The inset in Fig. 5(b) shows the responsivity versus intensity curve maintained almost linear.

In order to investigate the influence of thermal annealing on the performance of $ZnGa_2O_4$ based solar blind photodetectors, different DUV PDs were fabricated, where $ZnGa_2O_4$ epilayers were thermal annealed at 700, 800 and 900 °C in nitrogen ambient for 1 hour. The spectral responsivity of the annealed DUV PDs was measured and compared with those of as-grown $ZnGa_2O_4$ based PDs as illustrates in Fig. 5(c). It can be clearly observed that the variation of photoresponse properties of DUV PDs could be attributed to oxygen vacancies effects during the different temperature annealing process. For the ohmic-type PDs based on the as-grown and annealed at 700 °C, $ZnGa_2O_4$ epitaxial films presented no selectivity of responsivity in DUV region. On the contrary, the device based on the 800 °C annealing had a high rejection ratio of 104 from 240 nm to 320 nm band, as shown in Fig. 5(c). Furthermore, it decreases to 103 (not shown here) for 900 °C annealed $ZnGa_2O_4$ PDs devices. Thus 800 °C is the optimized annealing temperature used to fabricate the DUV PDs, which exhibited strong selectivity to solar blind radiation without interference with UV-A (320–400 nm) and visible radiation. The measured absolute peak responsivity for as-grown, 700 °C, 800 °C, and 900 °C annealed devices were 2782, 136.3, 86.3 and 0.007 A/W at 230 nm, respectively. Therefore, the PDs made of $ZnGa_2O_4$ epilayers annealed 900 °C can not be used as DUV PDs due to low responsivity. It was worthy to mention that the responsivity for the annealed $ZnGa_2O_4$ PDs devices dropped significantly (Fig. 5(c)), which is consistent to those reported in earlier studies[12,22]. Even though, the selectivity of the DUV PDs made of $ZnGa_2O_4$ annealed at 800 °C presents the highest for these DUV PDs. The detailed dark current (Idark) and UV-illuminated photocurrent (Ilight) at 230 nm I–V curves for MSM UPDs fabricated from as-grown and annealed (700, 800, 900 °C) $ZnGa_2O_4$ epitaxial films have been discussed in the Supporting Text (Supplementary information 2).

Moreover, no response was given to the UV-A/B, and almost 90% of peak intensity was obtained as the wavelength shorter than 280 nm for PDs made of 800 °C annealed $ZnGa_2O_4$. Therefore, the sharp cutoff and obviously high rejection power of this PD proved its potential as a candidate for solar-blind DUV detection application. Although the DUV PD made of as-grown $ZnGa_2O_4$ films presented such high responsivity of ~2782 A/W (under 230 nm DUV), the selectivity to spectral responsivity was too low to use. As-grown $ZnGa_2O_4$ films contained higher defects than those of annealed $ZnGa_2O_4$ films. The high responsivity was due to the defects in the as-grown films, which resulted in trapping states that can enhance internal gain. Zheng et al.[25] also demonstrated that the high responsivity of $Mg_{0.46}Zn_{0.54}O$ film-based detectors is attributed to the long life time of photo-ionized holes trapped in the deep level, as precisely measured using deep-level transient spectral technique. The long life time is commonly induced by the trap states of holes, which include the interface states between semiconductor and electrode, surface states, and deep level defects[14]. After furnace annealing, the responsivity of UVA region (310–400 nm) decreased by about three orders of magnitude for $ZnGa_2O_4$ film detectors. The spectral response of annealed $ZnGa_2O_4$-based detectors was in the range of 210–240 nm.

Response time is another important parameter to determine the suitability of detector for specific application. The response time is a measurement of the time required for photo signal to increase or decay to a specific value and defined as the time to reach 90% saturation response. Decay time is the time taken by the PDs to decay 10% of the maximum photocurrent when the UV light is switched off. The transient continuous photoresponse behavior of the as-grown and annealed $ZnGa_2O_4$ PDs was investigated under 230 nm DUV light with an intensity of ~62.5 μW/cm^2 and at a bias of 5 V. PDs were measured by periodically turning on and off the UV light. The rise and decay time at 5 V bias were more than 10 s for the as-grown $ZnGa_2O_4$ PDs, shown in the inset of Fig. 5(d). Correspondingly, the measured typical rise and decay time are 0.5 and 0.7 s, respectively, for the DUV PDs fabricated using annealed $ZnGa_2O_4$ films as shown in Fig. 5(d). Obviously, there exists the PPC effect in the as-grown $ZnGa_2O_4$ PDs. The PPC effect is a light-induced enhancement in the conductivity that persists for a long period after the termination of light excitation. It was resulted from the deep level traps. In the as-grown $ZnGa_2O_4$, the deep level traps comes from the oxygen vacancy and surface density states which could be demonstrated by CL, AFM and I-V characteristics. These results agreed well with recently published results about $ZnGa_2O_4$-based PDs[23,24,26]. On the other hand, there was no PPC effect and no noticeable change in photocurrent upon turning on and off the light illumination over multicycles for the annealed $ZnGa_2O_4$ PDs. This continuous variation in photocurrent of annealed $ZnGa_2O_4$ film PDs indicated excellent reproducibility and stability. Evidently, the annealing treatment alleviates the PPC effect[27]. Additionally, the complete response of as-grown and annealed (800 °C) $ZnGa_2O_4$ DUV PDs are presented in Fig. S3 (Supplementary Information 3).

Figure 6 displays the noise power density of $ZnGa_2O_4$ thin film with and without annealing at 5 V bias. The frequency range was tuned from 1 Hz to 1600 Hz. The obtained spectra from the PD can be fitted well by the Hooge-type equation as follows[28].

$$S_n(f) = S_o\left(\frac{I_d^\beta}{f^\alpha}\right),$$

where I_d is the dark current, f is the frequency, S_o is a constant, and α and β are two fitting parameters. The fitting curve of noise power density spectra for two $ZnGa_2O_4$ DUV PDs (Fig. 6) was similar to $1/f$ with the frequency at < 500 Hz. The pure $1/f$ noise indicated that the noises at <500 Hz were related to flicker noise. Flicker noise or $1/f$-type noise mainly originates from the acoustic phonons and ionized impurities that cause mobility fluctuation through lattice and impurity scatterings[29]. The noises at >500 Hz for as-grown $ZnGa_2O_4$ DUV PD decreased as $1/f^2$ due to generation-recombination noise. Obviously, generation-recombination noise can be reduced by thermal annealing due to the oxygen vacancy reducing. With these values, we can determine the constant S_o from Fig. 6. The So values for as-grown and annealed $ZnGa_2O_4$ DUV PDs were 1.70×10^{-7} and 1.3×10^{-7}, respectively. At a bandwidth (B) of 1000 Hz, the total square noise current $<in^2>$ can be estimated by integrating $S_n(f)$.

In general, we assume that $S_n(f) = S_n(1\,Hz)$ when $f < 1$ Hz. Thus, the noise equivalent power (NEP) and detectivity (D*) are given as follows.
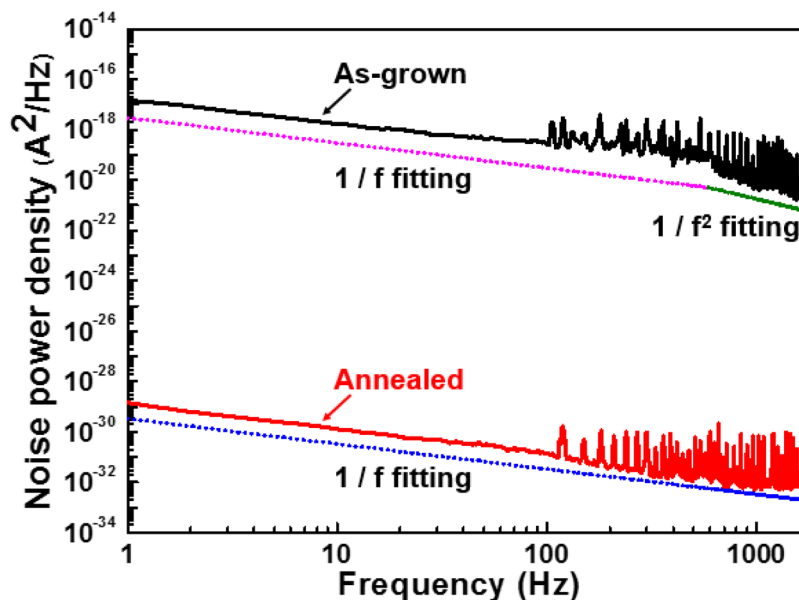
Figure 6. Noise power density of as grown and annealed $ZnGa_2O_4$ UPDs.

$$\langle in \rangle^2 = \int_0^B S_n(f)df = \int_0^1 S_n(1)df + \int_1^B S_n(f)df = S_o[\ln(B) + 1],$$

$$NEP = \frac{\sqrt{\langle in \rangle^2}}{R} \quad D* = \frac{\sqrt{A}\sqrt{B}}{NEP},$$

where R is the responsivity of the DUV PDs, and A and B are the active areas of the PD and the bandwidth. The NEP of as-grown and annealed $ZnGa_2O_4$ PDs was approximately 9.33×10^{-9} and 9.994×10^{-12} W, which corresponded to D* of 2.449×10^8 and 2.2870×10^{11} cm Hz $^{0.5}$ W^{-1}, respectively.

Moreover, Table S1 (Supplementary Information 4) shows the performance comparison with recently published ternary oxide-based PDs. Inadequate studies have been conducted on these types of PDs. The $ZnGa_2O_4$ thin-film PDs presented the potential to achieve the highest UV-to-visible ratio in the order of 10^7, lowest dark current of 1 pA, and short response time compared with those of other PDs based on MSM structure[30–36].

This result suggested that thermal annealing treatment increased the PD detectivity. Furthermore, the detectivity of annealed $ZnGa_2O_4$ thin film was suitable for PD application.

Discussion

We have successfully grown a single-crystalline $ZnGa_2O_4$ thin film on sapphire substrate by MOCVD techniques. The as-grown films exhibit the high density of oxygen vacancy defects and surface density states, which can result in deep trapping centers that increase the generation of current or trap-assisted leakage current. Consequently, the rise and decay times of as-grown PD devices are delayed, which is unsuitable for practical optoelectronic device application. However, the PD after annealing provides sufficient energy to reduce the oxygen vacancy defects and surface density states in as-grown samples to repair each other. After annealing treatment, $ZnGa_2O_4$ film shows good photoelectric characteristics. To date, no relevant research has been published yet about PD based on single-crystalline $ZnGa_2O_4$ thin films with sharp cutoff wavelength (280 nm), obviously high responsivity (86.3 A/W, under 230 nm DUV), considerably low dark current (<1 pA), short response time (<1 s), and high current on–off ratio (~10^7). Therefore, the $ZnGa_2O_4$ PD system is a high potential candidate for solar-blind UV detection application.

Experimental Method and Device Fabrication

$ZnGa_2O_4$ thin films were grown on c-plane (0001) sapphire substrates via a low-pressure MOCVD system. Diethyl zinc (DEZn), triethylgallium (TEGa), and oxygen (99.999%) were used as precursors. Ar (99.999%) was utilized as carrier gas to deliver DEZn and TEGa vapors to the reactor. The most excellent quality of the epilayer thin film was obtained at the low pressure of 15 Torr, growth temperature of 650 °C, and total growth time of 90 min. The flow rates of DEZn, TEGa, and oxygen were maintained at 40, 50, and 200 sccm, respectively. Previously, we have systematically investigated in details the effects of different growth parameters on the successfully grown (111)-oriented single-crystalline $ZnGa_2O_4$ films by MOCVD technique[11]. The as-grown epilayer was subsequently annealed in the furnace for 1 h at 700, 800 and 900 °C in nitrogen ambient. Crystalline quality and the epilayer orientation were measured using a high-resolution XRD (HR-XRD) system (PANalytical, X'Pert³ Pro MRD) with a Cu Kα line (λ = 1.541874 Å) as the radiation source. Ge (220) crystal was used as the monochromator. The surface roughness of as-grown and annealed $ZnGa_2O_4$ films was studied by atomic force

microscope. The chemical bonding states and surface compositions of $ZnGa_2O_4$ films were analyzed by XPS (ULVAC-PHIPHI 5000; monochromatic Al Kα radiation, 1486.6 eV). The atomic structure of $ZnGa_2O_4$ thin films was characterized using X-ray absorption near-edge structure (XANES) and extended X-ray absorption fine structure (EXAFS) spectroscopy of Ga K-edge. Ga spectra were obtained at a beamline of 17C1 at the National Synchrotron Radiation Research Center in Hsinchu, Taiwan. The energy bandgaps (E_g) of the $ZnGa_2O_4$ films were investigated by CL measurements. To measure the optoelectric characteristics of $ZnGa_2O_4$ films, Ti/Al/Ti/Au (50/1700/50/200 nm) electrodes with a width of 50 μm and intra-distance of 50 μm were patterned on top of the $ZnGa_2O_4$ films using photolithography. The ohmic metal was deposited by e-beam evaporation. Deuterium lamp (30 W) was used as DUV light source for photoresponse measurements. The semiconductor parameter analyzer (4155B, Keysight Technologies) was used to measure the current–voltage (I–V) characteristics of the fabricated devices in a dark ambient environment at room temperature. The schematic structure of an interdigitated finger PD with top electrodes is shown in Fig. S4 (Supplementary Information 5). In the measurement process of noise power density, the dark current was measured by precision semiconductor parameter analyzer (4156 C, Keysight Technologies) first. Then, the bias and sensitivity were set in the low noise current preamplifier (SR 570, Stanford Research Systems). Finally, the low-frequency noise from 1–1000 Hz was obtained by dynamic signal analyzer (35670 A, Keysight Technologies).

References

1. Ozbay, E. *et al.* High-performance solar-blind photodetectors based on Al/sub x/Ga/sub1-x/N heterostructures. *IEEE J. Quantum Electron.* **10**(4), 742–751 (2004).
2. Monroy, E., Omnès, F. & Calle, F. Wide-bandgap semiconductor ultraviolet photodetectors. *Semicond. Sci. Technol.* **18**(4), R33–R51 (2003).
3. Salem, A. A., Soliman, A. A. & El-Haty, I. A. Determination of nitrogen dioxide, sulfur dioxide, ozone, and ammonia in ambient air using the passive sampling method associated with ion chromatographic and potentiometric analyses. *Air Qual Atmos Health.* **2**(3), 133–145 (2009).
4. Chen, H., Liu, K., Hu, L., Al-Ghamdi, A. A. & Fang, X. New concept ultraviolet photodetectors. *Materialstoday.* **18**(9), 493–502 (2015).
5. Jung, Y. R. *et al.* Pt/AlGaN metal semiconductor ultra-violet photodiodes on crack-free AlGaN layers. Jpn. *J. Appl. Phys.* **42**(4B), 2349–235 (2003).
6. Sang, L. W., Liao, M. Y., Koide, Y. & Sumiya, M. High-temperature ultraviolet detection based on InGaN Schottky photodiodes. *Appl. Phys. Lett.* **99**, 031115:1–031115:3 (2011).
7. Feng, P., Zhang, J. Y., Li, Q. H. & Wang, T. H. Individual β-Ga₂O₃ nanowires as solar-blind photodetectors. *Appl. Phys. Lett.* **88**, 153107:1–153107:3 (2006).
8. Ravadgar, P. *et al.* Effects of crystallinity and point defects on optoelectronic applications of β-Ga₂O₃ epilayers. *Optics Express.* **21**(21), 24599–24610 (2013).
9. Li, C., Bando, Y., Liao, M., Koide, Y. & Golberg, D. Visible-blind deep-ultraviolet Schottky photodetector with a photocurrent gain based on individual Zn₂GeO₄ nanowire. *Appl. Phys. Lett.* **97**, 161102–3 (2010).
10. Shen, Y. S., Wang, W. K. & Horng, R. H. Characterizations of Metal-Oxide-Semiconductor Field-Effect Transistors of ZnGaO Grown on Sapphire Substrate. *IEEE J. Of the Elec. Devices Soc.* **5**(2), 112–116 (2017).
11. Horng, R.-H., Huang, C. Y., Ou, S. –L., Juang, T.-K. & Liu, P. –L. Epitaxial Growth of ZnGa₂O₄: A New, Deep Ultraviolet Semiconductor Candidate. *Cryst. Growth Des.* **17**(11), 6071–6078 (2017).
12. Alema, F. *et al.* Solar blind photodetector based on epitaxial zinc doped Ga2O3 thin film. *Phys. Status Solidi A.* **214**(S), 1600688:1–7 (2017).
13. Omata, T., Ueda, N., Ueda, K. & Kawazoea, H. New ultraviolet-transport electroconductive oxide, ZnGa₂0₄ spinel. *Appl. Phys. Lett.* **64**, 1077–1078 (1994).
14. Han, S. *et al.* Photoconductive gain in solar-blind ultraviolet photodetector based on Mg₀.₅₂Zn₀.₄₈O thin film. *Appl. Phys. Lett.* **99**, 242105–4 (2011).
15. Huang, C. Y., Horng, R. H., Wu, D. S., Tu, L. W. & Kao, H. S. Thermal annealing effect on material characterizations of β−Ga₂O₃ epilayer grown by metal organic chemical vapor deposition. *Appl. Phys. Lett.* **102**, 011119:1–011119:3 (2013).
16. Guo, D. Y. *et al.* Unipolar resistive switching behavior of amorphous gallium oxide thin films for nonvolatile memory applications. *Appl. Phys. Lett.* **106**, 042105–4 (2015).
17. Kim, J. H. *et al.* Correlation of the change in transfer characteristics with the interfacial trap densities of amorphous In–Ga–Zn–O thin film transistors under light illumination. *Appl. Phys. Lett.* **98**, 232102 (2011).
18. Guo, D. Y. *et al.* Oxygen vacancy tuned Ohmic-Schottky conversion for enhanced performance in β-Ga₂O₃ solar-blind ultraviolet photodetectors. *Appl. Phys. Lett.* **105**, 023507–4 (2014).
19. Wang, Z. *et al.* Tuning the selectivity toward CO evolution in the photocatalytic conversion of CO₂ with H₂O through the modification of Ag-loaded Ga₂O₃ with a ZnGa₂O₄ layer. *Catalysis Science & Technology.* **6**, 1025–1032 (2016).
20. Behrens, P., Kosslick, H., Tuan, V. A., Fröba, M. & Neissendorfer, F. X-ray absorption spectroscopic study on the structure and crystallization of Ga-containing MFI-type zeolites. *Microporous Materials.* **3**, 433–441 (1995).
21. Criado, G. M. *et al.* Crossed Ga₂O₃/SnO₂ Multiwire Architecture: A Local Structure Study with Nanometer Resolution. *Nano letters.* **14**, 5479–5487 (2014).
22. Li, Y. B. *et al.* Efficient assembly of bridged β-Ga₂O₃ nanowires for solar-blind photodetection. *Adv. Funct. Mater.* **20**, 3972–3978 (2010).
23. Singh, K., Rawal, I., Punia, R. & Dhar, R. X-ray photoelectron spectroscopy investigations of band offsets in Ga0.02Zn0.98O/ZnO heterojunction for UV photodetectors. *J. Of Appl. Phys.* **122**, 155301:1–155301:13 (2017).
24. Lou, Z., Li, L. & Shen, G. High-performance rigid and flexible ultraviolet photodetectors with single-crystalline ZnGa₂O₄ nanowires. Nano. *Research.* **8**(7), 2162–2169 (2015).
25. Zheng, Q. *et al.* High-Responsivity Solar-Blind Photodetector Based on Mg₀.₄₆Zn₀.₅₄O Thin Film. *IEEE Elec. Dev. Lett.* **33**(7), 1033–1035 (2012).
26. Feng, P., Zhang, J. Y., Wan, Q. & Wang, T. H. Photocurrent characteristics of individual ZnGa₂O₄ nanowires. *J. of Appl. Phys.* **102**, 074309–4 (2007).
27. Tebano, A., Fabbri, E., Pergolesi, D., Balestrino, G. & Traversa, E. Room-Temperature Giant Persistent Photoconductivity in SrTiO₃/LaAlO₃ Heterostructures. *Acs Nano.* **6**(2), 1278–1283 (2012).
28. Chuanga, M. Y. *et al.* Density-controlled and seedless growth of laterally bridged ZnO nanorod for UV photodetector applications. *Sensors and Actuators B.* **202**, 810–819 (2014).
29. Chang, S. J. *et al.* GaN-Based Schottky Barrier Photodetectors With a 12-Pair MgxNy–GaN Buffer Layer. *IEEE J. of Quantum Electron.* **44**(10), 916–920 (2008).

30. Feng, H. *et al.* Fabrication and UV-sensing properties of one-dimensional β-Ga$_2$O$_3$ nanomaterials. *Phys. Status Solidi A.* **210**, 1861–1865 (2013).
31. Zhang, M. *et al.* NaTaO3-Based Ultraviolet Photodetector With Capacitive Efficacy. *IEEE Elec. Dev. Lett.* **34**, 1539–1541 (2013).
32. Zhao, Y. *et al.* Ultraviolet Photodetector Based on a MgZnO Film Grown by Radio-Frequency Magnetron Sputtering. *ACS Applied Mater. & Interface.* **1**(11), 2428–2430 (2009).
33. Zhang, M. *et al.* Ultraviolet Detector Based on SrZr0.1Ti0.9O3 Film. *IEEE Elec. Dev. Lett.* **34**(3), 420–422 (2013).
34. Zhang, M. *et al.* High response solar-blind ultraviolet photodetector based on Zr$_{0.5}$Ti$_{0.5}$O$_2$ film. *Appl.Surf. Sci.* **268**, 312–316 (2013).
35. Xing, J., Changchun, Z., Erjia, G. & Yang, F. High-Performance Ultraviolet Photodetector Based on Polycrystalline SrTiO$_3$ Thin Film. *IEEE Sens. J.* **12**(8), 2561–2564 (2012).
36. Li, L. *et al.* Ultrahigh-performance solar-blind photodetectors based on individual single-crystalline In2Ge2O7 nanobelts. *Adv. Mater.* **22**, 5145–5149 (2010).

Acknowledgements

Author Contributions

T., S.H. conceived and designed the experiments. B., S. analyzed the data and wrote the manuscript. H., C.Y. contributed to grow the ZnGa$_2$O$_4$ films by MOCVD. H., L.C. measured the X-ray absorption fine structure (EXAFS) spectra of ZnGa$_2$O$_4$ film. L., Y.G. analyzed the EXAFS data. H., R.H. designed experiments, analyzed, verified the data and wrote the manuscript. All authors read and approved the final version of the manuscript to be submitted.

Additional Information

Supplementary information accompanies this paper at https://doi.org/10.1038/s41598-018-32412-3.

Competing Interests: The authors declare no competing interests.

Publisher's note: Springer Nature remains neutral with regard to jurisdictional claims in published maps and institutional affiliations.